A multichannel radiometric profiler of temperature, humidity, and cloud liquid

Randolph Ware,[1] Richard Carpenter,[2] Jürgen Güldner,[3] James Liljegren,[4] Thomas Nehrkorn,[5] Fredrick Solheim,[1] and Francois Vandenberghe[6]

Received 11 December 2002; revised 23 February 2003; accepted 28 March 2003; published 31 July 2003.

[1] A microwave radiometer is described that provides continuous thermodynamic (temperature, water vapor, and moisture) soundings during clear and cloudy conditions. The radiometric profiler observes radiation intensity at 12 microwave frequencies, along with zenith infrared and surface meteorological measurements. Historical radiosonde and neural network or regression methods are used for profile retrieval. We compare radiometric, radiosonde, and forecast soundings and evaluate the accuracy of radiometric temperature and water vapor soundings on the basis of statistical comparison with radiosonde soundings. We find that radiometric soundings are equivalent in accuracy to radiosonde soundings when used in numerical weather forecasting. A case study is described that demonstrates improved fog forecasting on the basis of variational assimilation of radiometric soundings. The accuracy of radiometric cloud liquid soundings is evaluated by comparison with cloud liquid sensors carried by radiosondes. Accurate high-resolution three-dimensional water vapor and wind analysis is described on the basis of assimilation of simulated thermodynamic and wind soundings along with GPS slant delays. Examples of mobile thermodynamic and wind profilers are shown. Thermodynamic profiling, particularly when combined with wind profiling and slant GPS, provides continuous atmospheric soundings for improved weather and dispersion forecasting. *INDEX TERMS:* 6969 Radio Science: Remote sensing; 3394 Meteorology and Atmospheric Dynamics: Instruments and techniques; 0694 Electromagnetics: Instrumentation and techniques; 3329 Meteorology and Atmospheric Dynamics: Mesoscale meteorology; *KEYWORDS:* microwave radiometer, thermodynamic profiling, weather forecasting

Citation: Ware, R., R. Carpenter, J. Güldner, J. Liljegren, T. Nehrkorn, F. Solheim, and F. Vandenberghe, A multichannel radiometric profiler of temperature, humidity, and cloud liquid, *Radio Sci.*, *38*(4), 8079, doi:10.1029/2002RS002856, 2003.

1. Introduction

[2] A radiometric profiler that provides temperature and humidity soundings up to 10 km height and low-resolution cloud liquid soundings is described by *Solheim et al.* [1998] and by *Güldner and Spänkuch* [2001]. The radiometric profiler is shown in Figure 1. The radiometer observes radiation intensity at 12 frequencies in a region of the microwave spectrum that is dominated by atmospheric water vapor, cloud liquid water, and molecular oxygen emissions. Microwave observation frequencies at 22.035, 22.235, 23.835, 26.235, 30.0, 51.25, 52.28, 53.85, 54.94, 56.66, 57.29, and 58.8 GHz were chosen by eigenvalue analysis to optimize profile retrieval accuracy [*Solheim and Godwin*, 1998]. The radiometer observes within in an inverted cone with a 2–3 degree beamwidth at 51–59 GHz, and 5–6 degree beamwidth at 22–30 GHz. The radiometric profiler includes zenith infrared and surface temperature, humidity and pressure sensors.

[3] The water vapor absorption line at 22 GHz is pressure broadened with a magnitude that decreases with height. By observing radiated power at selected frequencies in this region the water vapor profile can be

[1]Radiometrics Corporation, University Corporation for Atmospheric Research, Boulder, Colorado, USA.
[2]Weather Decision Technologies Inc., Norman, Oklahoma, USA.
[3]Meteorological Observatory, German Weather Service, Lindenberg, Germany.
[4]Argonne National Laboratory, Argonne, Illinois, USA.
[5]Atmospheric and Environmental Research Inc., Lexington, Massachusetts, USA.
[6]National Center for Atmospheric Research, Boulder, Colorado, USA.

0048-6604/03/2002RS002856$11.00

Figure 1. Radiometric profiler (Radiometrics TP/WVP-3000) with 12 microwave and 1 infrared observation channels.

determined. The molecular oxygen absorption band is relatively strong, limiting observed emission at 60 GHz to several hundred meters above the radiometer. Moving away from band center, the absorption decreases and emission can be observed at increasing height. By observing radiated power at a number of frequencies in the oxygen band, the temperature profile can be determined. Liquid water emission in the microwave spectrum increases approximately with the frequency squared. Low-resolution cloud liquid profiles can be determined by observing radiated power at selected frequencies from 22 to 59 GHz, together with a cloud base height measurement. Cloud base height is estimated from zenith infrared observations of cloud base temperature and the retrieved temperature profile.

[4] Historical radiosondes at sites representative of the observing location are used with neural network or regression methods to retrieve tropospheric profiles from the microwave, infrared, and surface meteorological measurements. Use of radiosonde statistics significantly enhances retrieval accuracy and resolution beyond the levels suggested by eigenvalue analysis of the microwave observations alone [*Solheim et al.*, 1996]. Retrieval output is set to 100 m levels from the surface to 1 km and to 250 m levels from 1 to 10 km, for a total of 47 levels. The presence of cloud liquid is assumed in neural network training at levels where radiosonde sensed relative humidity (RH) is above a threshold amount. A range of cloud liquid amounts from zero to 0.8 g/m^3 are assumed [*Decker et al.*, 1978] for neural network training. Neural network retrievals are based on forward modeling of ~10,000 radiosonde soundings using radiative transfer equations [*Schroeder and Westwater*, 1991], and a standard back propagation algorithm. Atmospheric absorption models for oxygen and water vapor used in the radiative transfer equations are discussed by *Liljegren et al.* [2001a]. Specific locations of radiosondes used for neural network training are identified for each example discussed below. Neural network methods are discussed by *Solheim et al.* [1998]. Regression methods are discussed by *Güldner and Spänkuch* [2001]. Regression retrievals based on radiosondes are expected to provide better agreement with radiosondes since they avoid forward modeling and calibration errors inherent in neural network retrievals. *Westwater* [1993] provides references to microwave radiometric profiling work.

[5] In the following sections we discuss radiometric profiler accuracy and reliability, compare radiometric, radiosonde and forecast soundings, and compare radiometric and balloon-based cloud liquid soundings. Mobile thermodynamic and wind profiling systems with applications in high-resolution mesoscale forecasting are

described, along with advanced radiometric profile assimilation methods. Finally, we summarize results demonstrating high-resolution three-dimensional wind and water vapor analysis based on simulated slant delay observations from a Global Positioning Satellite (GPS) network combined with continuous wind and thermodynamic soundings.

2. Accuracy and Reliability

[6] The radiometer K-band channels (22–30 GHz) are calibrated by tipping [*Han and Westwater*, 2000]. The V-band (51–59 GHz) calibration uses a patented cryogenic blackbody target. Tipping and cryogenic calibrations are automatically transferred to a temperature stabilized noise source. An internal mirror points to any elevation angle and an azimuth drive enables pointing to any sky direction. Radiated power observations at the various frequencies are converted to brightness temperatures using Planck's law [*Han and Westwater*, 2000]. Brightness temperatures are used as inputs for neural network or regression retrievals. Instrument accuracy in sensing brightness temperatures is 0.5 K rms. Radiometric profile accuracy has been determined by statistical comparison with radiosondes at Lindenberg, Germany [*Güldner and Spänkuch*, 2001]; Barrow, Alaska, and Lamont, Oklahoma [*Liljegren et al.*, 2001b, 2001c]. The radiometer design has proven its reliability in locations including the Arctic, midlatitudes, and the tropics. Additional information on radiometer design and performance is available via http://radiometrics.com.

3. Example Observations

[7] Radiometric profilers have been operated in a variety of locations and weather conditions. Example retrievals are presented from Lindenberg, Germany, and U.S. locations in Colorado, Oklahoma, and New Hampshire. All of the example retrievals are based on neural network training. Accuracies of neural network and regression retrievals based on statistical comparison with radiosondes at Lindenberg are also presented. Zenith infrared and surface meteorological measurements are included in the neural network retrievals. Surface meteorological measurements are included in the regression retrievals.

3.1. Lindenberg, Germany

[8] The German Weather Service (Deutscher Wetterdienst (DWD)) is evaluating the use of wind and thermodynamic profilers for use in operational forecasting. Time series including 1, 3 and 7 days of neural network retrievals are routinely produced by DWD as part of the evaluation. The retrievals are based on Lindenberg radiosondes. An example 3-day time series is shown in Figure 2. Frontal passage including relatively

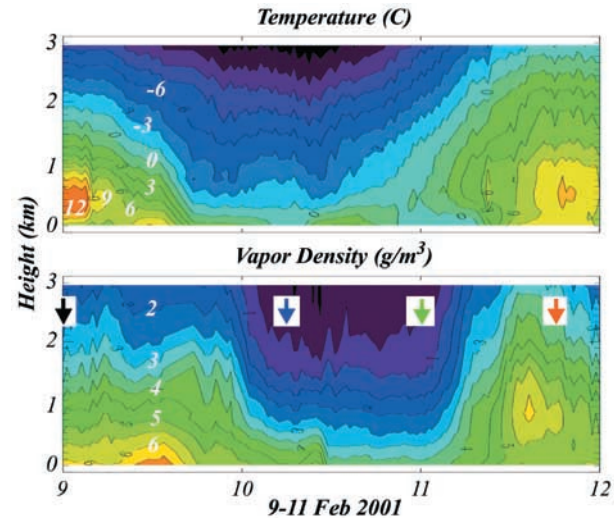

Figure 2. Time series of radiometric temperature and humidity soundings up to 3 km height at Lindenberg, Germany, 9–11 February 2001. Arrows mark radiosonde launch times. Radiosonde and radiometric soundings are compared in the following figure.

cold, dry air occurred during this 3-day period. A 6°C temperature inversion at 500 m height disappeared during the first several hours of the first day, and a general cooling trend continued until late in the day. On the second day, a gradual warming trend started around midday and continued through midday on the third day, with development of a 1–2°C temperature inversion at 500 m height. Relatively high levels of vapor density held during most of the first day, with rapid drying occurring toward the end of the day. The second day remained relatively dry. Early on the third day, vapor density began to increase, reaching a maximum value of 6 g/m^3 at 1 km height around midday. Vapor density gradually decreased later in the day.

[9] Single radiometric soundings immediately before and after the radiosonde launch times (with a 9-min sampling interval) are shown on a logarithmic height scale in Figure 3. The plots are truncated at 3 km because variability in temperature and water vapor density is minimal above this height during the time period shown. Relatively cold dry air was observed on the second day (blue) with the temperature decreasing by 7–12 K below 500 m height, relative to the first day (black), and the average vapor density decreasing by ~2.0 g/m^3 below 2 km height. A 5–6°C temperature inversion at 400–500 m height is seen at 0000 UTC on 9 February (black) in the radiosonde and radiometric soundings. A smaller, 2–4°C temperature inversion at 600–1000 m height, and a 1–2 g/m^3 water vapor maximum at 1 km height, are seen at 18 UTC on 11 February (red). The radiosonde

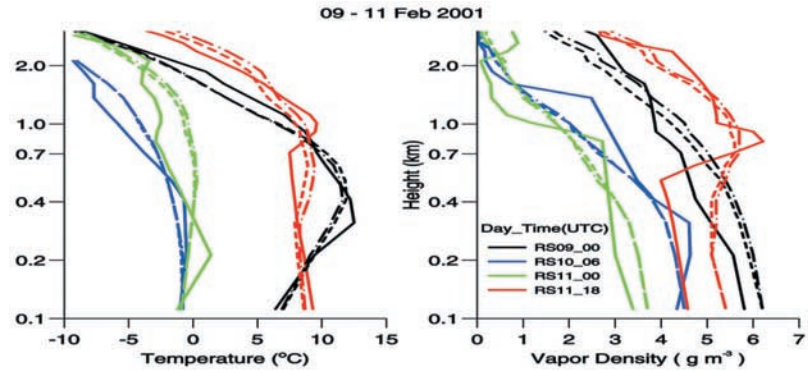

Figure 3. Radiosonde (solid) and radiometric soundings (logarithmic height scale) at Lindenberg corresponding to the times of the colored arrows in the previous figure. Single radiometric soundings immediately before (dashed) and after (dot-dash) the radiosonde launch time are also shown.

shows a minor 2–3°C temperature inversion at 200 m height at 0000 UTC on 11 February (green), and the radiometer retrievals show a 1°C temperature inversion at 500 m height. Sounding differences are consistent with the high vertical resolution of radiosonde point measurements and the lower vertical resolution of the radiometer volumetric measurements.

[10] Statistical comparisons of simultaneous radiosonde soundings and radiometer neural network and regression retrievals are shown in Figure 4. Included are comparisons with several hundred radiosondes launched at six hour intervals during winter and summer months by the German Weather Service at Lindenberg, Germany [*Güldner and Spänkuch*, 2001]. Also shown are radiosonde errors (http://lnx21.wwb.noaa.gov/oberr/reanl-obs.html) used by the National Centers for Environmental Prediction (NCEP) when assimilating radiosonde soundings into numerical weather models. The NCEP radiosonde errors are dominated by "representativeness error," the error generated in characterization of model cell volumes by point measurements. For example, a radiosonde measurement of 100% RH in a small cloud within a model cell volume would poorly represent a cell with a significantly lower average RH value. Representativeness error can be reduced or eliminated by using volumetric measurements, instead of point measurements, to define average cell volume RH values. Even if perfect agreement were found between the

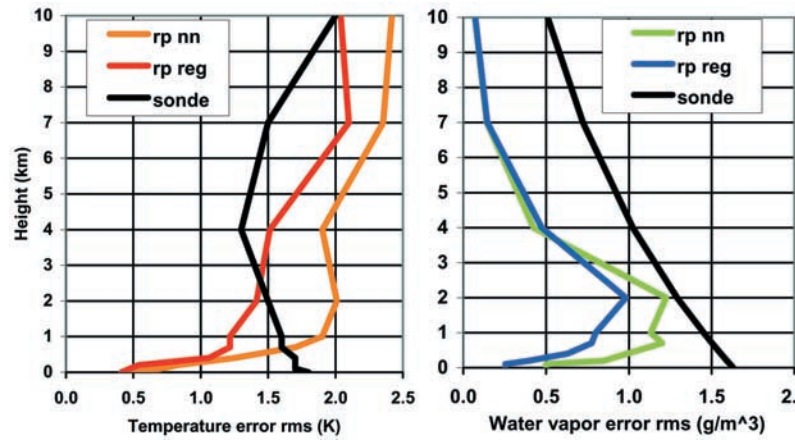

Figure 4. Radiometric profile retrieval accuracy based on statistical comparison with radiosonde soundings. Radiosonde (sonde) errors are provided by NCEP. Root mean square (rms) differences between radiosondes and radiometer retrievals based on neural network (nn) and regression (reg) are shown.

radiometer retrievals and radiosonde soundings, this would not imply that the retrieval is more accurate than the radiosonde, but only of equal accuracy.

[11] Neural network retrievals include calibration and line shape errors. Calibration by tipping in the K-band [*Han and Westwater*, 2000], and by observation of a liquid nitrogen target in the V-band, can achieve 0.5 K accuracy. However, larger errors can be generated by tipping calibration when gradients of atmospheric water vapor or cloud liquid are present. Retrievals based on regression of simultaneous radiometric brightness temperature and radiosonde observations are not affected by calibration and line shape errors. The regression retrievals shown in Figure 4 are based on 237 simultaneous radiosonde and radiometer soundings during summer and 254 during winter at Lindenberg [*Güldner and Spänkuch*, 2001]. As expected, regression retrieval errors are smaller than neural network retrieval errors. For temperature soundings, the regression retrieval error is smaller than the radiosonde error below 2.5 km height, and the neural network retrieval error is smaller than the radiosonde error below 600 m; above these heights radiosonde error is smaller than radiometer retrieval error. For water vapor density soundings, the regression and neural network retrieval errors are smaller than the radiosonde error at all heights.

[12] Differences ranging from -0.1 to $+0.9$ g/m^3 between the radiometer and radiosonde surface water vapor measurements (-2 to +17% in relative humidity) are seen in Figure 3. The radiosonde launch site at Lindenberg is located in an open graveled area one hundred meters away from the radiometer observation location on top of a three-story building surrounded by large trees. High temporal and spatial variability in water vapor may account for these differences. The differences shown are smaller than the 1.5 g/m^3 error for radiosonde surface water vapor density measurements shown in Figure 4, and the 2 g/m^3 maximum error for radiosonde surface water vapor density measurements reported by *Wang et al.* [2002]. It is evident in Figure 3 that the radiometer soundings are smoother than the radiosonde soundings. This occurs because the radiometer observes a volume of air in an inverted cone subject to a vertical weighting function [*Westwater*, 1993], and the radiosonde provides a point measurement. In general, we conclude from Figure 4, and from similar statistical results reported by *Liljegren et al.* [2001b, 2001c] at Arctic and south central U.S. observation sites, that radiometric soundings are roughly equivalent in accuracy to radiosonde soundings when used in numerical weather modeling.

3.2. Boulder, Colorado

[13] Radiometric neural network retrievals are compared in Figure 5 with mesoscale forecasts during the onset of upslope weather conditions at Boulder, Colorado. Supercooled fog conditions associated with the upslope continued for four days, causing diversion of several hundred flights from Denver International Airport. Neural network training used Denver radiosondes launched from a site 50 km southeast of Boulder. Cloud base height was calculated using infrared measurement of cloud base temperature combined with the retrieved temperature profile. Cloud top was assumed as the height where the RH profile decreased to 80%. Cloud shape and integrated liquid were determined by the neural network. A numerical simulation was performed using the Mesoscale Model version 5 (MM5) (see http://www.mmm.ucar.edu/mm5). Twelve hour forecasts were initialized at 0000 UTC and 1200 UTC on 16 February 2001 using a 10-km horizontal grid with 27 vertical levels. The MM5 forecast did not predict fog in the Denver basin. However, regional fog was accurately forecast by MM5 after variational assimilation of the Boulder radiometric soundings [*Vandenberghe and Ware*, 2003].

[14] The retrieved and forecast temperature, relative humidity, and liquid profiles in Figure 5 are significantly different. For example, the forecast temperature is up to 5 K colder than the retrieval at 1 km height until 1100 UTC, and warmer by the same amount after 1800 UTC. In addition, the RH forecast shows saturation above 4 km height after 1600 UTC, whereas the retrieval shows saturation below 300 m after 1200 UTC. Similarly, cloud liquid is forecast after 1600 UTC at 4–9 km height, whereas the retrieval shows cloud below 1 km height after 1200 UTC.

[15] Radiometric retrievals at Boulder are compared with simultaneous radiosonde profiles at Denver in Figure 6. The temperature profiles agree within several degrees K up to 8 km height, and both soundings show a 4–7 K inversion at 1 km height. The largest disagreement occurs at 8.7 km height, where the radiosonde detects a sharp minimum associated with the tropopause, whereas the retrieval shows a gradual decrease in lapse rate suggesting a tropopause height near 10 km. The profiles agree within 10% RH up to 7 km height, decreasing to agreement within $\sim$20% RH above this level. The radiosonde at Denver shows RH near saturation below 300 m height that is consistent with the presence of fog from the surface to 400 m in the Boulder retrieval. The Boulder retrieval also shows high values of RH and the presence of cloud liquid from the surface to 400 m, with a maximum density of 0.3 g/m^3 at 200 m height. This case study illustrates the value of continuous radiometric profiling for airport weather applications including measurement and prediction of fog, supercooled liquid, and the vertical extent of cloud liquid water.

3.3. Lamont, Oklahoma

[16] Radiometric neural network retrievals are compared in Figure 7 with mesoscale forecasts during early

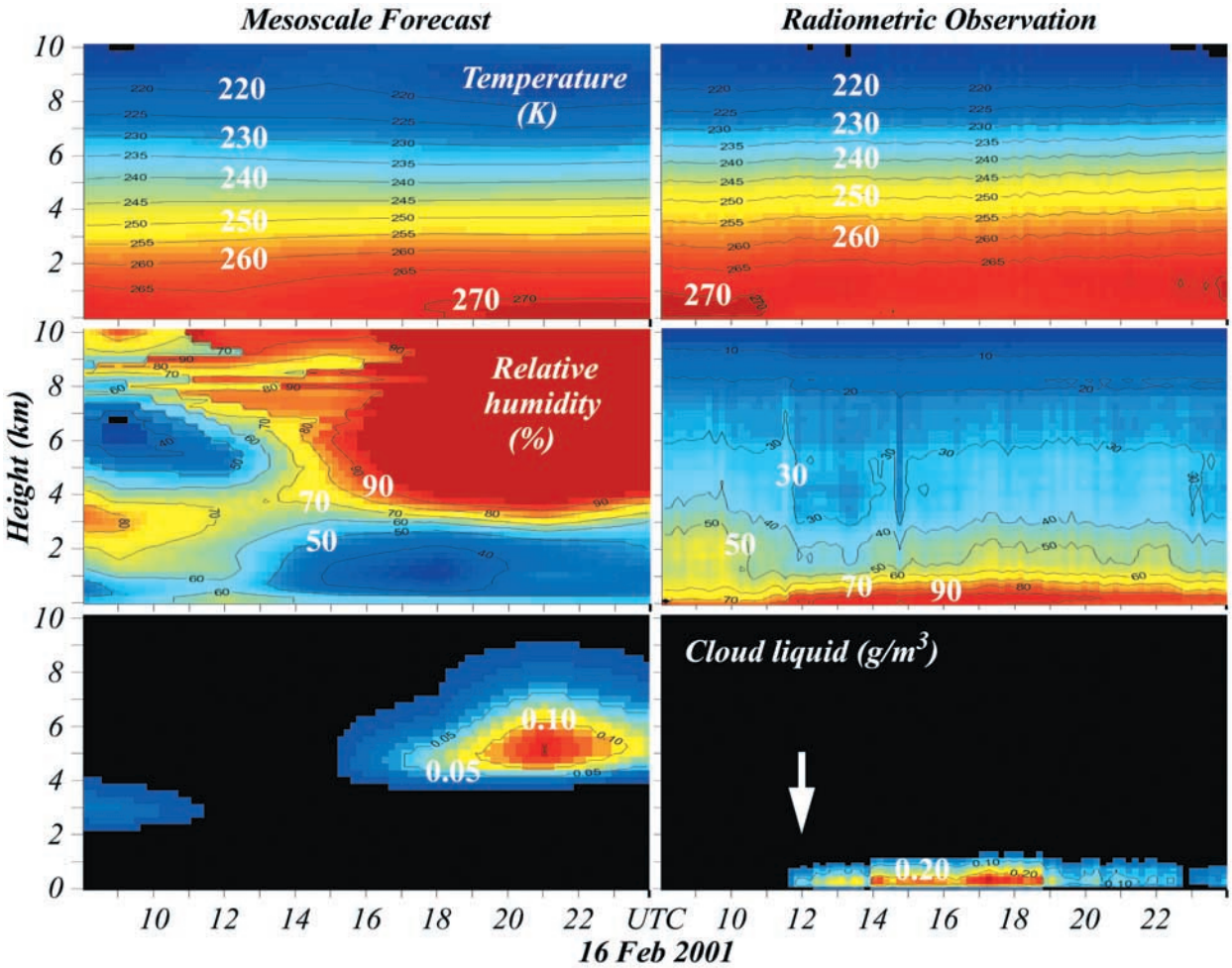

Figure 5. Forecast (3-hour) and radiometric temperature, relative humidity and cloud liquid profiles at Boulder, Colorado, 16 February 2001. Maximum forecast and observed cloud liquid densities are 0.15 and 0.3 g/m^3, respectively. The radiometer detected fog that was not forecast. Radiosonde launch time is marked by the arrow.

spring weather conditions in Oklahoma. Neural network training was based on radiosondes launched at the Department of Energy's Atmospheric Radiation Measurement (ARM) Program's Southern Great Plains Central Facility located 10 km southwest of Lamont, Oklahoma. The radiometric profiler was located within 1 km of the radiosonde launch site.

[17] A 24-hour numerical simulation was performed using the Advanced Regional Prediction System (ARPS) (see http://www.caps.ou.edu/ARPS). The forecast was initialized at 1200 UTC 21 Mar 2000 using a 24-km horizontal grid with 64 vertical levels. Satellite measurements of cloud top and ceilometer measurements of cloud base were assimilated into ARPS. The radiometric soundings indicate the presence of low clouds throughout the 24-hour period, except for a few hours centered around 0000 UTC 22 Mar 2000. The ARPS forecast is considerably warmer and drier at low levels, and hence shows less cloudiness. At 1 km height the accuracy of the neural network temperature retrieval is better than 2 K, and it is likely that the temperature and humidity retrievals are more accurate than the numerical forecast.

[18] The high variability in retrieved RH seen in Figure 7 from 3 to 7 km height may be induced by finite "shutter speed," the time interval for serial observations at 12 microwave frequencies. The retrieval model assumes that the same atmosphere is observed at all frequencies. During variable cloud conditions, observed brightness temperatures can vary by several degrees K over time intervals of 1 min or less. As a result, retrieval accuracy can be degraded. The shutter speed for all examples discussed in this paper was 72 s; it has subsequently been

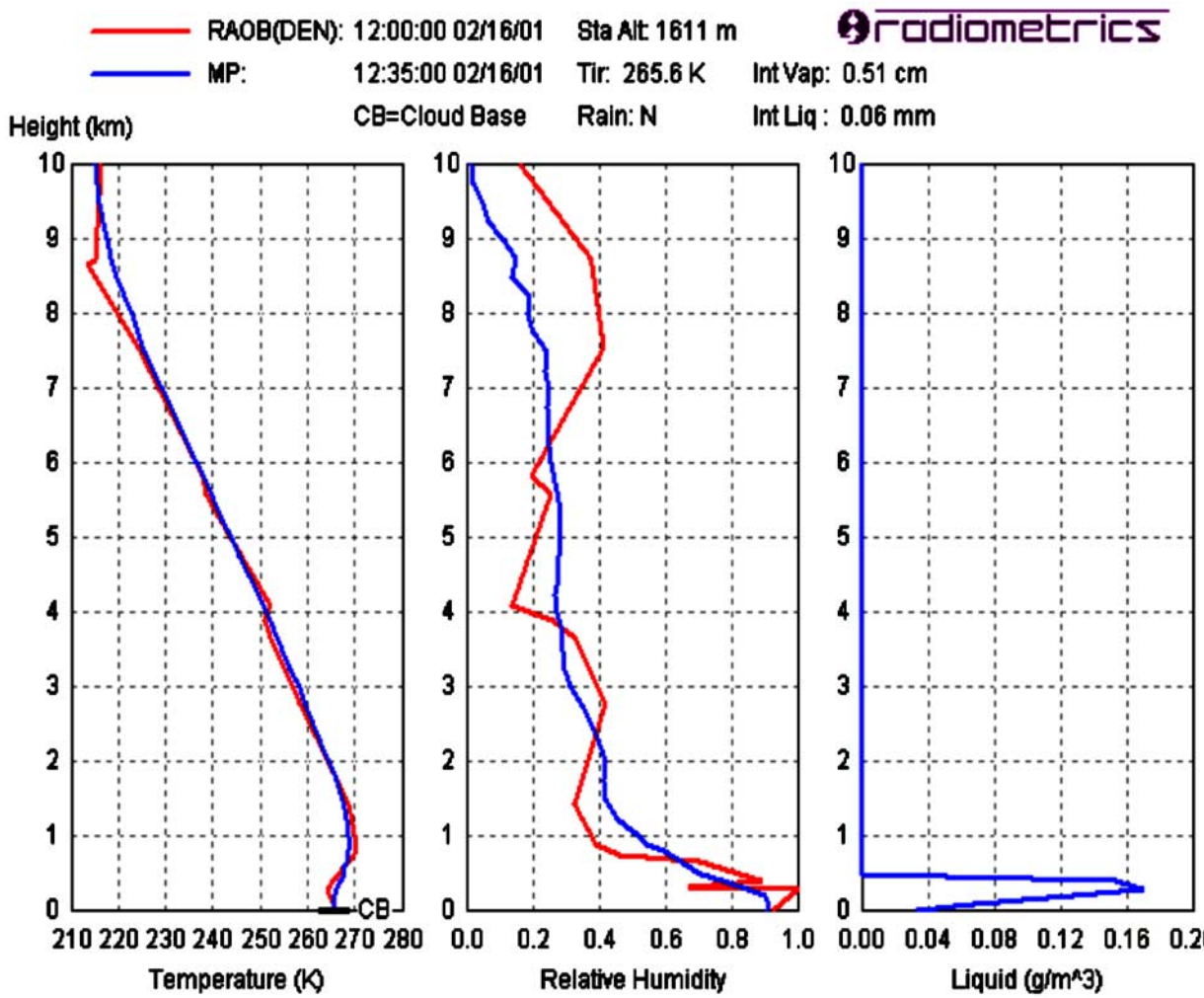

Figure 6. Radiosonde soundings at Denver (red) and radiometer soundings at Boulder (blue), just after the onset of supercooled fog conditions. The Denver radiosonde site is 50 km southeast of the radiometer site at Boulder. The cloud liquid (fog) profile retrieved from radiometer observations is shown in the right-hand panel.

reduced to 20 s to minimize retrieval error associated with finite shutter speed.

[19] An example comparison of radiosonde and radiometric soundings is shown in Figure 8. Temperature (T) and dewpoint (DP) soundings are shown in the left-hand panel, along with cloud base temperature observed by the zenith infrared sensor (T_{IR}). The intersection of T_{IR} with the temperature profile provides an estimate of cloud base height. In this case, T_{IR} and the temperature profile intersect around 2 km height. If a temperature inversion is present, the cloud base height estimate can be ambiguous. However, ambiguity can often be resolved using the retrieved RH profile. RH soundings and the maximum possible RH (limited by saturation over ice for temperatures below 0°C) are shown in the center panel. The right-hand panel shows vapor and liquid density profiles, amounts of precipitable water (PW) determined by radiosonde and radiometer, and liquid water path (LWP) determined by the radiometer. Dewpoint, RH, and water vapor density plots contain redundant information that is included to provide units familiar to a variety of users. Additional radiometric and radiosonde sounding comparisons are available for Lamont, Oklahoma, and Barrow, Alaska [*Liljegren et al.*, 2001b].

4. Cloud Liquid Profiles

[20] The radiometric profiler provides low-resolution liquid soundings of one cloud layer. To validate this capability, radiometer and radiosonde cloud liquid

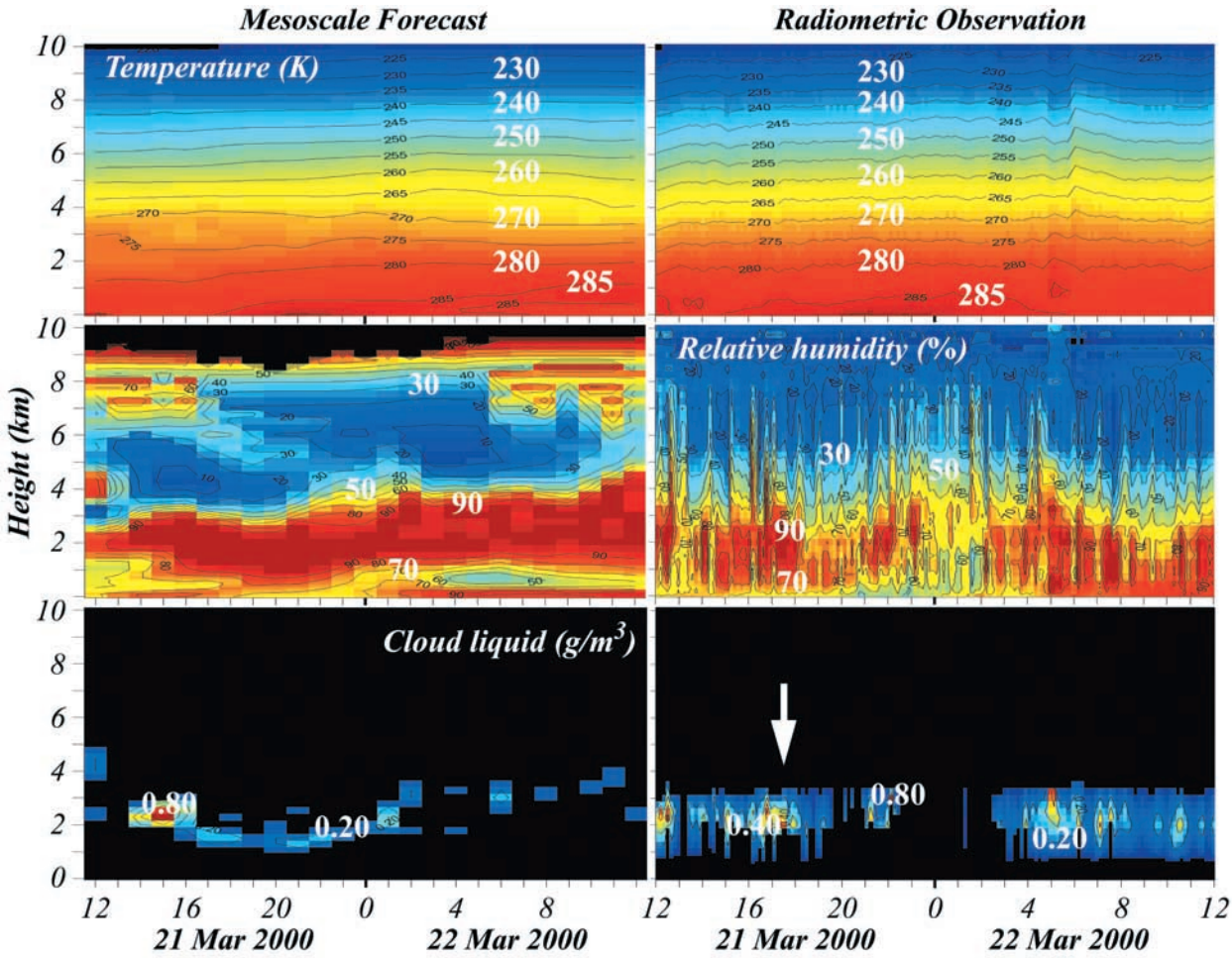

Figure 7. Forecast and radiometric temperature, relative humidity, and cloud liquid profiles at Lamont, Oklahoma, on 21–22 March 2000. Radiosonde launch time is marked by the arrow. Maximum forecast and observed cloud liquid densities are 1 g/m^3.

soundings were obtained during April 1999 in New Hampshire during the Mount Washington Icing Sensors Project (MWISP) (see http://www2.faa.gov/aua/awr/mwisp). The balloons carried vibrating wire sensors that measure supercooled cloud liquid water density with an accuracy estimated at ~50% [*Hill*, 1996]. Radiometric cloud liquid profiles were calculated as follows: (1) cloud base height was set to the lowest height where the cloud base temperature measurement is equal to the retrieved temperature profile, (2) cloud top height was set to the height where the radiometric RH profile decreases to 90%, (3) a triangular cloud shape was chosen with the apex at the height where the radiometric RH profile reached its maximum value, and (4) the integrated cloud liquid in the profile was adjusted to equal the integrated liquid value retrieved by the neural network.

[21] Adiabatic and rectangular cloud shapes were also calculated. However, the triangular cloud shape provided better agreement, on average, with the radiosonde soundings. Neural network training was based on radiosondes from Albany, NY. The Albany radiosonde launch site altitude is 94 m and the Mt. Washington observation site altitude is 811 m. To adjust for the height difference, Albany radiosonde observations below 811 m were omitted from neural network training. A total of 24 simultaneous balloon and radiometric soundings were compared, selecting the radiometer observation time closest to the balloon launch time. The three best and three worst cases of agreement between the two methods are shown in Figure 9. Agreement was estimated as ratio of the overlapping areas of the profiles divided by the average area of the two profiles. For example, ~90%

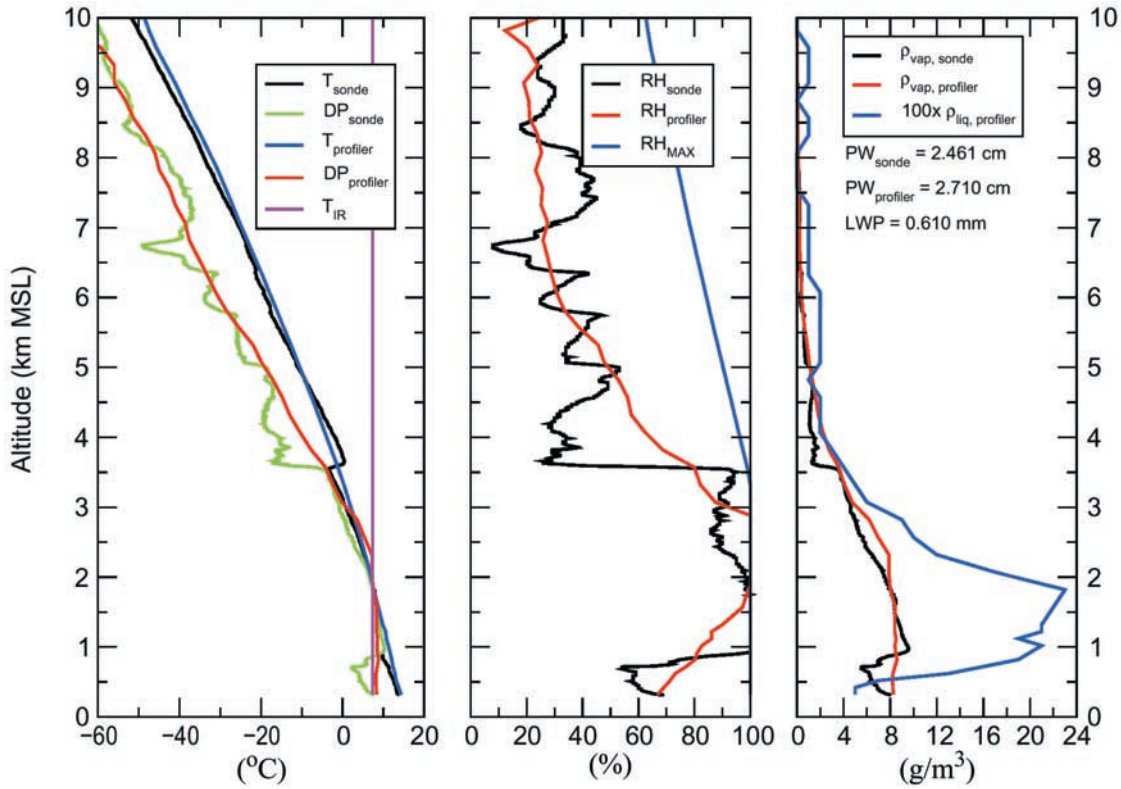

Figure 8. Comparison of radiosonde and radiometric soundings near Lamont, Oklahoma, 21 March 2000, 17:31 UTC. The radiometric cloud liquid retrieval is also shown.

agreement is seen in the upper left panel, and ~10% agreement is seen in the lower left panel.

[22] The comparison experiment was limited by the following: (1) synchronization of the two sensing methods was limited by the 10 min sampling cycle of the radiometer, (2) the same atmosphere was often not observed by the two methods as wind typically carried the balloon out of the field of view of the radiometer, and (3) the balloon-based sensor made a point measurement of liquid water in a supercooled state only, whereas the radiometer made a volumetric measurement of liquid in all states, in an inverted cone with a beamwidth less than or equal to 6 degrees. In spite of these limitations, the average agreement between the two methods is approximately 50% for the 24 cases, equal to the estimated accuracy of the supercooled liquid sensor. The integrated liquid water measurements were also compared. The radiometer minus the radiosonde integrated liquid water average for all 24 cases is 0.16 mm, with 0.13 mm standard deviation. Radiometer sensitivity to liquid water at all temperatures, compared to the sensitivity of the balloon-based sensor only to liquid water at temperatures below freezing, may account for the positive bias in the radiometer minus radiosonde comparison.

[23] These results briefly demonstrate the capability for continuous sounding of cloud liquid by radiometric profilers. The radiometer can also measure spatial variations in cloud liquid by elevation angle scanning, as reported by *Liljegren* [1999]. Continuous monitoring of supercooled liquid and the vertical extension of cloud liquid is useful for airport weather applications. Other applications for continuous cloud liquid sounding include weather modification, initialization of cloud liquid in numerical weather models, cloud physics research, and studies of climate-related radiative transfer.

5. Wind and Thermodynamic Profiling Plus Slant GPS

[24] Short term (1–12 hours) weather forecasting skill is notoriously poor [*Emanuel et al.*, 1995; *Dabberdt and Schlatter*, 1996; *Wilson et al.*, 1998]. Although reasonably accurate forecasts can be obtained one hour ahead, forecast skill rapidly degrades until initialization with new radiosonde observations, typically 12 hours later. This situation can be improved using continuous wind and thermodynamic soundings that respond to short term

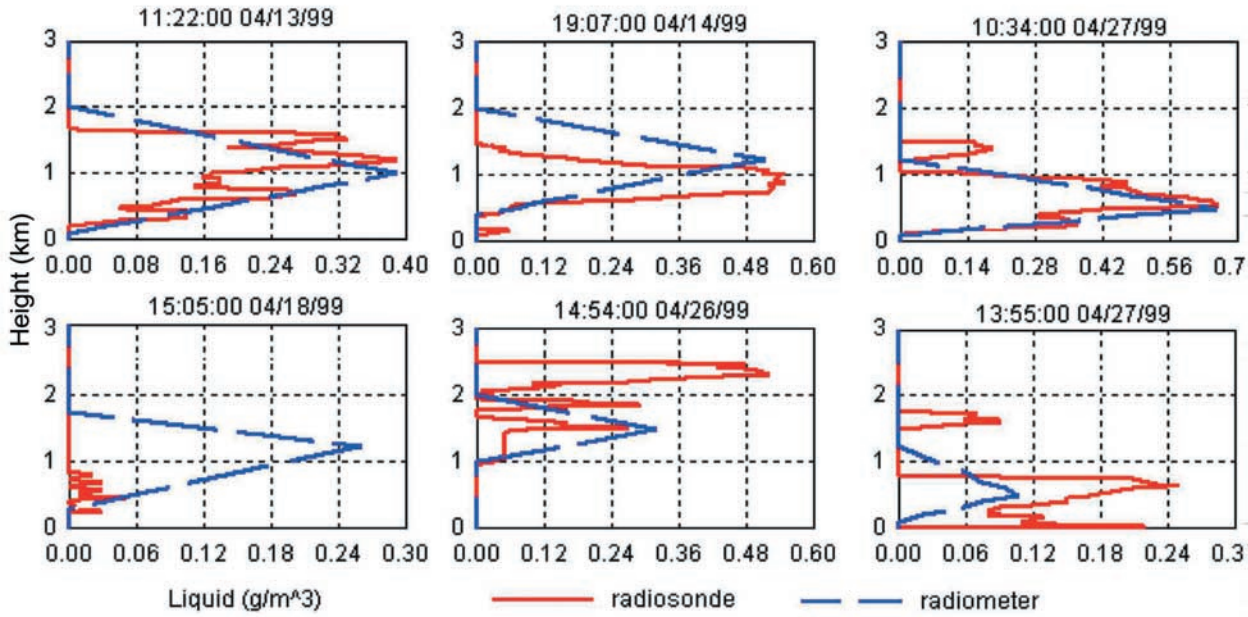

Figure 9. Balloon-based and radiometric soundings of cloud liquid at Mt. Washington, New Hampshire (1999). Six cases from a set of 24 comparisons are shown, including the three best (upper) and three worst (lower) levels of agreement between the two sounding methods.

changes in upper air. In addition to wind soundings, wind radar signal to noise measurements contain information on the height and strength of refractivity gradients [*Stankov et al.*, 2003; *Nash et al.*, 2003]. Refractivity gradient information can be used to improve the vertical resolution of radiometric soundings. Further improvements are expected if raw radiometric (brightness temperatures) and wind radar (moments) measurements are directly assimilated into models [*Ware et al.*, 2002]. Combined thermodynamic and wind profiling systems are shown in Figure 10. The systems shown are mobile, allowing rapid deployment for weather research and forecasting [*Knupp*, 2003]. Applications include short term convection, precipitation, and dispersion forecasting for airports, space launch ranges, power plants, construction projects, and outdoor sporting

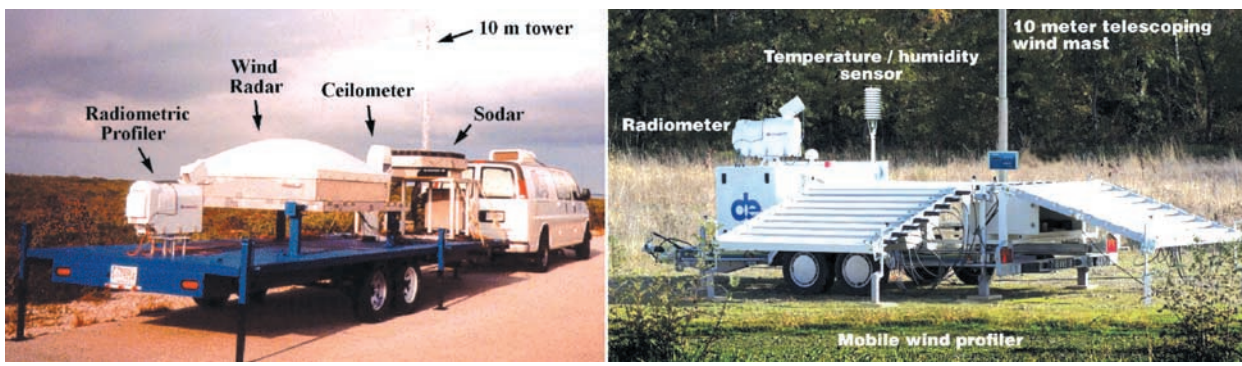

Figure 10. Mobile systems designed for research (left) (see http://vortex.nsstc.uah.edu/mips) and commercial applications (right) (see http://www.meteo.degreane.fr) including radiometric and wind profilers. Both mobile profilers include 10 m wind sensing masts. A ceilometer and sodar are included in the research mobile profiler.

events. High-resolution forecasting can be used to mitigate hazards from atmospheric dispersion of dangerous materials.

[25] Local forecast improvements can be extended to regional scales by assimilating signal delays from Global Positioning System (GPS) networks. Delays induced by atmospheric density and water vapor along the ray paths of Global Positioning System (GPS) signals can be accurately measured [*Ware et al.*, 1997; *Braun et al.*, 2003]. These slant delays provide strong horizontal constraints on atmospheric moisture and mass fields for numerical weather analysis [*MacDonald and Xie*, 2003]. For example, three-dimensional water vapor analysis identifying the location and magnitude of convective storms was obtained using three-dimensional variational assimilation (3DVAR) of simulated GPS slant wet delays and radiometric water vapor soundings [*MacDonald et al.*, 2002]. In addition, significant improvements in precipitation threat scores were obtained by assimilating simulated slant GPS observations into a mesoscale model [*Ha et al.*, 2003].

[26] High-resolution winds can also be recovered if wind profiler observations and total GPS slant delays are included in the 3DVAR analysis [*MacDonald et al.*, 2001]. At elevation angles below 2 degrees, GPS slant delays are accurate to 1% or better [*Pany*, 2002]. Slant delays at these low-elevation angles extend for distances of 100 km or more in the boundary layer. These low-angle slant delays can be used to extend local constraints obtained from continuous thermodynamic and wind soundings to regional scales [*Ware et al.*, 2003]. The potential of wind and thermodynamic profiling combined with slant GPS has stimulated planning by the National Oceanic and Atmospheric Administration (NOAA) for a U.S. National MesoNet including 1000 GPS sites, and 120 wind and thermodynamic profiling sites [*MacDonald and Xie*, 2003]. Investigation of the potential for regional wind, thermodynamic and GPS observation networks is also underway in Europe and Asia. Results of investigations on this topic were reported at the International Workshop on GPS Meteorology, 14–17 January 2003, in Tsukuba, Japan (see http://www.mri-jma.go.jp/Workshop/gpsmet).

6. Conclusions

[27] Radiometric profiling provides continuous temperature and humidity soundings up to 10 km height in clear and cloudy conditions, and low-resolution cloud liquid soundings. The accuracy of the radiometric temperature and humidity soundings is equivalent in accuracy to radiosonde soundings when used in numerical weather forecasting. Comparison with numerical weather forecasts shows that significant short term temperature and moisture field variations are detected by radiometric profiling that are not forecast. In one case study, variational assimilation of radiometric soundings provided accurate prediction of significant upslope supercooled fog that was missed by forecasts with no radiometric assimilation. Cloud liquid soundings retrieved from radiometric profiler observations were compared with soundings from supercooled cloud liquid sensors carried by radiosondes. Agreement of 50% was found, in spite of spatial/temporal sampling differences, and comparison of all liquid measurements to supercooled liquid only measurements. Mobile wind and thermodynamic profiling systems can provide flexibility in obtaining continuous wind and thermodynamic soundings for research and weather and dispersion forecasting. Forecast improvements are expected if raw radiometric and wind profiler measurements are assimilated. By also assimilating slant delays from GPS networks, the location and magnitude of major convective storms can be predicted. Recognizing the potential for this new approach, several national forecast organizations are evaluating and planning combined wind, thermodynamic and GPS networks to improve severe weather and high-resolution dispersion forecasting.

[28] **Acknowledgments.** The authors acknowledge the support of DOE contract DE-FG03-96ER82266 (W. Ferrell, Project Officer), NASA contract NAS-01005 (A. Reehorst, Program Manager) and Army Research Laboratory contract DAAD17-01-C-0045 (E. Measure, Program Manager), and helpful guidance from E. Westwater, J. Vivekanandan, and anonymous reviewers.

References

Braun, M., C. Rocken, and J. Liljegren, Comparisons of line-of-sight water vapor observations using the global positioning system and a pointing microwave radiometer, *J. Atmos. Oceanic Technol.*, *20*, 606–612, 2003.

Dabberdt, W., and T. Schlatter, Research opportunities from emerging atmospheric observing and modeling capabilities, *Bull. Am. Meteorol. Soc.*, *77*, 305–323, 1996.

Decker, M., E. Westwater, and F. Guiraud, Experimental evaluation of ground-based microwave radiometric sensing of atmospheric temperature and water vapor profiles, *J. Appl. Meteorol.*, *17*, 1788–1795, 1978.

Emanuel, K., et al., Report of the First Prospectus Development Team of the U.S. Weather Research Program to NOAA and the NSF, *Bull. Am. Meteorol. Soc.*, *76*, 1194–1208, 1995.

Güldner, J., and D. Spänkuch, Remote sensing of the thermodynamic state of the atmospheric boundary layer by ground-based microwave radiometry, *J. Atmos. Oceanic Technol.*, *18*, 925–933, 2001.

Ha, S.-Y., Y.-H. Kuo, Y.-R. Guo, and G.-H. Lim, Variational assimilation of slant-path wet delay measurements from a hypothetical ground-based GPS network, *Mon. Weather Rev.*, in press, 2003.

Han, Y., and E. Westwater, Analysis and improvement of tipping calibration for ground-based microwave radiometers, *IEEE Trans. Geosci. Remote Sens.*, *38*, 1260–1276, 2000.

Hill, G., Analysis of supercooled liquid water measurements using microwave radiometer and vibrating wire devices, *J. Atmos. Oceanic Technol.*, *11*, 1242–1252, 1996.

Knupp, K., Mobile Integrated Profiling System (MIPS) observations of boundary layer and water vapor variations around boundaries and storms, in paper presented at 12th Symposium on Meteorological Observations and Instrumentation, Long Beach, Calif., Am. Meteorol. Soc., Boston, Mass., 10–13 Feb. 2003.

Liljegren, J., Observations of integrated water vapor and cloud liquid water at SHEBA, paper presented at 9th Atmospheric Radiation Measurement Program Science Team Meeting, San Antonio, Tex., Dep. of Energy, Washington, D. C., 22–26 March 1999.

Liljegren, J., E. Clothiaux, G. Mace, S. Kato, and X. Dong, A new retrieval for cloud liquid water path using a ground-based microwave radiometer and measurements of cloud temperature, *J. Geophys. Res.*, *106*, 14,485–14,500, 2001a.

Liljegren, J., E. Clothiaux, S. Kato, B. Lesht, F. , Initial evaluation of profiles of temperature, water vapor and cloud liquid water from a new microwave profiling radiometer, paper presented at 5th American Meteorological Society (AMS) Symposium on Integrated Observing Systems, Albuquerque, N. M., Am. Meteorol. Soc., Boston, Mass., 14–19 Jan. 2001b. (Available at http://radiometrics.com/ams01.pdf.)

Liljegren, J., B. Lesht, S. Kato, and E. Clothiaux, Initial evaluation of profiles of temperature, water vapor, and cloud liquid water from a new microwave profiling radiometer, paper presented at 11th Atmospheric Radiation Measurement (ARM) Program Science Team Meeting, Atlanta, Ga., Dep. of Energy, Washington, D. C., 19–23 March 2001c. (Available at http://radiometrics.com/MWRP_ARM01.pdf.)

MacDonald, A., and Y. Xie, On the use of GPS slant delay to recover three-dimensional meteorological fields, paper presented at International Workshop on GPS Meteorology, Min. of Education, Cult., Sports, Sci. and Technol., Jpn. Int. Sci. and Technol. Exch. Cent., Tsukuba, Japan, 14–17 Jan. 2003.

MacDonald, A., Y. Xie, and R. Ware, Use of a network of surface GPS receivers to recover three dimensional temperature and moisture, paper presented at IAMAS 2001 Assembly, Int. Assoc. of Meteorol. and Atmos. Sci., Innsbruck, Austria, July 2001.

MacDonald, A., Y. Xie, and R. Ware, Diagnosis of three dimensional water vapor using slant observations from a GPS network, *Mon. Weather Rev.*, *130*, 386–397, 2002.

Nash, J., T. Oakley, and C. Gaffard, Progress in improving upper air moisture measurements over the UK, paper presented at 12th Symposium on Meteorological Observations and Instrumentation, Long Beach, Calif., Am. Meteorol. Soc., Boston, Mass., 2003.

Pany, T., Measuring and modeling the slant wet delay with GPS and the ECMWF NWP model, *Phys. Chem. Earth*, *27*, 101–107, 2002.

Schroeder, J., and E. Westwater, User's guide to WPL microwave radiative transfer software, *NOAA Tech. Memo. ERL WPL-213*, Natl. Oceanic and Atmos. Admin., Silver Spring, Md., 1991.

Solheim, F., and J. Godwin, Passive ground-based remote sensing of atmospheric temperature, water vapor, and cloud liquid profiles by a frequency synthesized microwave radiometer, *Meteorol. Z.*, *7*, 370–376, 1998.

Solheim, F., J. Godwin, and R. Ware, Microwave radiometer for passively and remotely measuring atmospheric temperature, water vapor, and cloud liquid water profiles, *Final Contract Rep. DAAL01-96-2009*, White Sands Missile Range, White Sands, N. M., 1996. (Available at http://radiometrics.com/eigenvalue.pdf.)

Solheim, F., J. Godwin, E. Westwater, Y. Han, S. Keihm, K. Marsh, and R. Ware, Radiometric profiling of temperature, water vapor, and liquid water using various inversion methods, *Radio Sci.*, *33*, 393–404, 1998.

Stankov, B., E. Gossard, B. Weber, R. Lataitis, A. White, D. Wolfe, and D. Welsh, Humidity gradient profiles from wind profiling radars using the NOAA/ETL Advance Signal Processing System (SPS), *J. Atmos. Oceanic Technol.*, *20*, 3–22, 2003.

Vandenberghe, F., and R. Ware, Four-dimensional variational assimilation of ground-based microwave observations during a winter fog event, paper presented at International Workshop on GPS Meteorology, Min. of Education, Cult., Sports, Sci. and Technol., Jpn. Int. Sci. and Technol. Exch. Cent., Tsukuba, Japan, 14–17 Jan. 2003.

Wang, J., H. Cole, D. Carlson, E. Miller, and K. Beierle, Corrections of humidity measurement errors from the Vaisala RS80 Radiosonde—Application to TOGA COARE Data, *J. Atmos. Oceanic Technol.*, *19*, 981–1002, 2002.

Ware, R., C. Alber, C. Rocken, and F. Solheim, Sensing integrated water vapor along GPS ray paths, *Geophys. Res. Lett.*, *24*, 417–420, 1997.

Ware, R., F. Solheim, and F. Vandenberghe, Advanced assimilation of thermodynamic and wind soundings (abstract), presented at Workshop on COST 720: Integrated Ground-Based Remote Sensing Stations for Atmospheric Profiling, Eur. Coop. in the Field of Sci. and Tech. Res., Eur. Union, L'Aquila, Italy, 18–21 June 2002. (Available at http://radiometrics.com/pubs.)

Ware, R., J. Braun, S.-Y. Ha, D. Hunt, Y.-H. Kuo, C. Rocken, M. Sleziak, Van T. Hove, J. Weber, and R. Anthes, Real time water vapor sensing with SuomiNet—Today and tomorrow, paper presented at International Workshop on GPS Meteorology, Min. of Education, Cult., Sports, Sci. and Technol., Jpn. Int. Sci. and Technol. Exch. Cent., Tsukuba, Japan, 14–17 Jan. 2003.

Westwater, E., Ground-based microwave remote sensing of meteorological variables, in *Atmospheric Remote Sensing*

by Microwave Radiometry, edited by M. Janssen, chap. 4, pp. 145–213, John Wiley, New York, 1993.

Wilson, J., N. Crook, C. Mueller, J. Sun, and M. Dixon, Nowcasting thunderstorms: A status report, *Bull. Am. Meteorol. Soc.*, *79*, 2079–2099, 1998.

R. Carpenter, Weather Decision Technologies Inc., 1818 W Lindsey St., Building D, Suite 232, Norman, OK 73069, USA. (rcarpenter@wdtinc.com)

J. Güldner, Deutscher Wetterdienst, Meteorologisches Observatorium Lindenberg, Am Observatorium 12, D-15848 Tauche OT Lindenberg, Germany. (juergen.gueldner@dwd.de)

J. Liljegren, Argonne National Laboratory, 9700 S. Cass Avenue, Argonne, IL 60439, USA. (liljegren@anl.gov)

T. Nehrkorn, Atmospheric and Environmental Research Inc., 131 Hartwell Ave., Lexington, MA 04241-3126, USA. (tnehrkor@aer.com)

F. Solheim and R. Ware, Radiometrics Corporation, 2840 Wilderness Place #G, Boulder, CO 80301, USA. (solheim@radiometrics.com; ware@radiometrics.com)

F. Vandenberghe, National Center for Atmospheric Research, Boulder, CO 80307, USA. (vandenb@ucar.edu)